Accepted Manuscript

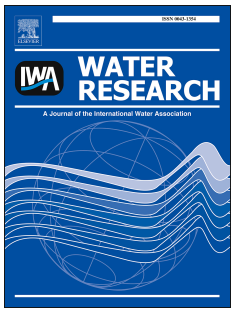

Bromate inhibition by reduced graphene oxide in thermal/PMS process

Xin Huang, Xujie Zhou, Jizhi Zhou, Zhifeng Huang, Shuang Liu, Guangren Qian, Naiyun Gao

PII: S0043-1354(17)30516-X

DOI: 10.1016/j.watres.2017.06.041

Reference: WR 12996

To appear in: *Water Research*

Received Date: 7 March 2017

Revised Date: 13 June 2017

Accepted Date: 14 June 2017

Please cite this article as: Huang, X., Zhou, X., Zhou, J., Huang, Z., Liu, S., Qian, G., Gao, N., Bromate inhibition by reduced graphene oxide in thermal/PMS process, *Water Research* (2017), doi: 10.1016/j.watres.2017.06.041.

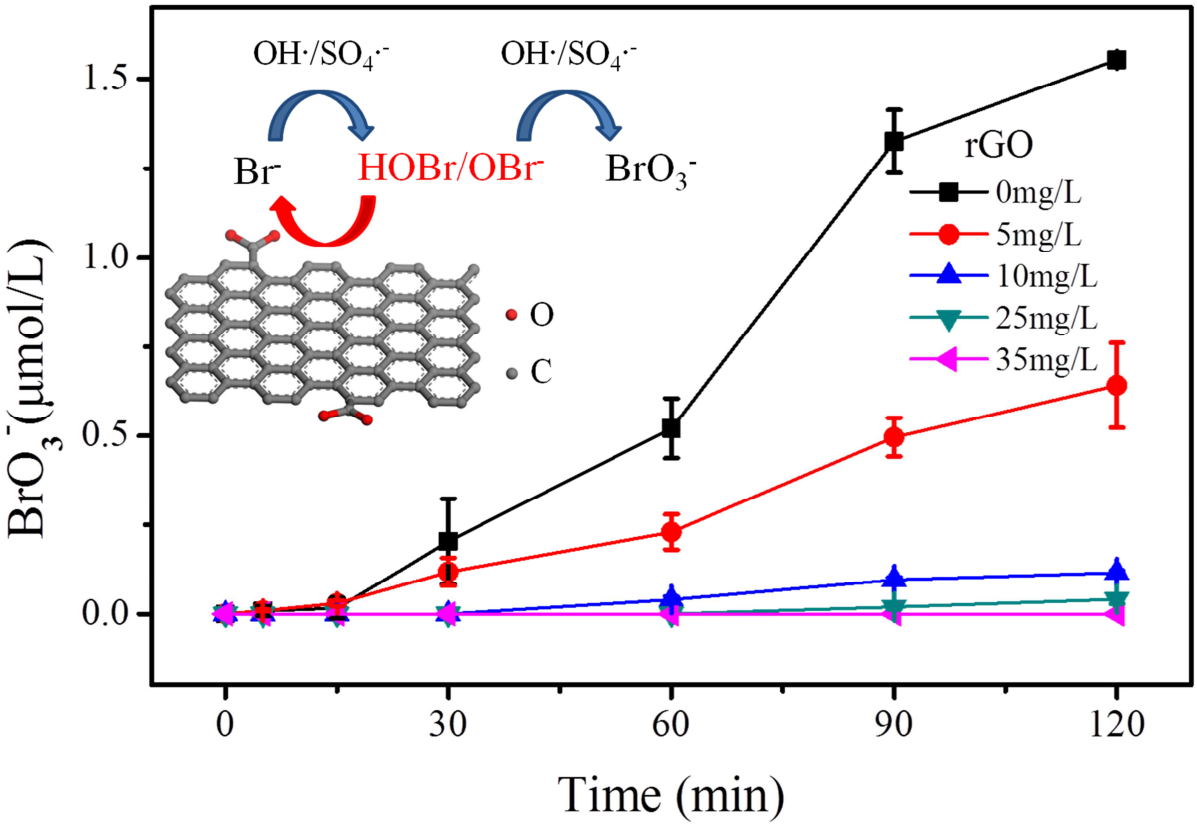

Bromate Inhibition by Reduced Graphene Oxide in Thermal/PMS Process

Xin Huang[a], *Xujie Zhou*[a], *Jizhi Zhou*[a,*], *Zhifeng Huang*[a], *Shuang Liu*[a], *Guangren Qian*[a], *Naiyun Gao*[b]

[a]School of Environmental and Chemical Engineering, Shanghai University, Shanghai 200444, China

[b]State Key Laboratory of Pollution Control and Resource Reuse, Tongji University, Shanghai 200092, China

* Corresponding author

*Tel: 086-021-66137748; Fax: 021-66137761; Email: jizhizhou@shu.edu.cn

Abstract: Bromate (BrO_3^-), as a contaminant producing from bromide (Br^-) oxidation, has been revealed for generation in sulfate radical involved processes. In this work, reduced graphene oxide (rGO) was firstly applied to inhibit the formation of BrO_3^- in thermally activated peroxymonosulfate (thermal/PMS) treatment. In the presence of 5 - 35 mg/L rGO, the decomposition rate of PMS was slightly increased from 0.0162 $\pm$ 0.0013 min^{-1} to 0.0200 $\pm$ 0.0010 min^{-1}, corresponding to removal rate of target pollutant increasing from 0.0157 $\pm$ 0.0012 min^{-1} to 0.0204 $\pm$ 0.0022 min^{-1}. This suggested the decay of PMS, the concentration and distribution of radicals were not influenced dramatically by the addition of rGO, which was partly supported by the almost unchanged HPLC chromatograms as compared with that in the absence of rGO. However, the produced BrO_3^- was significantly lowered by 67% - 100% with the

addition of rGO in a wide range of pH at 5 - 9 and activation temperature at 60 - 80 °C. Moreover, a quick reduction of hypobromous acid (HOBr) to Br^- was achieved with addition of rGO at room temperature, whilst no abatement of BrO_3^- and Br^- was observed in the same conditions. Therefore, masking HOBr was probably the role of rGO on bromate inhibition in thermal/PMS process. Because HOBr is a requisite intermediate for BrO_3^-, the inhibition effect of rGO is likely irrelevant of oxidation processes, which was inevitably showed by the good performance of rGO on BrO_3^- suppress in ozonation. Therefore, the addition of rGO in tens of mg/L is a promising measure to avoid the formation of unwanted bromine species in advanced oxidation processes.

Keywords: Graphene; Bromate; Persulfate; Sulfate radical

1. Introduction

Bromate (BrO_3^-) is one of disinfection by-products (DBPs) in water treatment. Because of its carcinogenicity and genotoxic property (Bull et al., 2012; Bulter et al., 2005), bromate is regulated at a maximum contaminant level of 10 μg/L in drinking water standards of many countries. Bromate is typically generated from bromide ion during ozonation process (Hofmann and Andrews, 2007). In recent years, researches showed that bromate can also be generated in non-ozone involved treatments such as ultraviolet combined with persulfate process (UV/persulfate), UV/chlorine and CuO-catalytic chlorination (Fang and Shang, 2012; Huang et al., 2008; Liu et al., 2012), which consequently hinder the application of those processes in the field of

drinking water treatment.

To minimize the formation of bromate in advanced oxidation processes, the masking of hypobromous acid (HOBr/BrO^-) seems a more practical option than others, such as removing bromide in source waters, lowering HO radical exposure at acidic pH, etc (Soltermann et al., 2017). HOBr has been proved as an important intermediate in bromate formation (Fang and Shang, 2012; Von Gunten and Hoigne, 1994). Briefly, bromide is first oxidized by oxidants and radicals to hypobromous acid, and then further oxidized to bromate. Therefore, dosing chemicals that could react with hypobromous acid quickly, i.e. H_2O_2 ($k_{OBr\cdot,H2O2}$ = (1.2 ± 0.2) × 10^6 M^{-1} s^{-1}, $k_{HOBr\text{-},HO2^-}$ = (7.6 ± 1.3) × 10^8 M^{-1} s^{-1}) and NH_3 ($k_{HOBr,NH3}$ = (4.0 - 7.5) × 10^7 M^{-1} s^{-1}), has been proved to be an effective way to suppress the formation of bromate and brominated organic compounds well (Berne et al., 2004; Von Gunten and Oliveras, 1997). Similar mechanisms on bromate inhibition occurred in heterogeneous catalysis systems as well. In nano-metal and cerium incorporated MCM-48 catalyzed ozonation, bromate was effectively minimized. The authors ascribed it to the decomposition of dissolved O_3 into OH radicals, which rapidly generated H_2O_2, and reduced HOBr to Br^- (Li et al., 2015; Wu et al., 2014). However, along with the effective quenching of HOBr, H_2O_2 accelerate the degradation of ozone and probably reduce the oxidation efficiency. In the case of dosing ammonia, formed bromamine that is similar as chloramine, facilitate the formation of unwanted N-DBPs, i.e. NDMA in suitable conditions (Le Roux et al., 2012).

Besides, some researches noticed the abatement of HOBr from heterogeneous

reaction. Nie et al. found that the reduction of HOBr by $MnOx/Al_2O_3$ were partly responsible for the inhibition of BrO_3^- forming over $MnOx/Al_2O_3$ with ozone (Nie et al., 2013). Note, carbon materials are the most historical and commonly used materials for reduction of bromate, i.e. powder and granular activated carbon (Bao et al., 1999; Huang and Cheng, 2008; Siddiqui et al., 1996). Because the standard redox potential of bromate/bromide ($E^{\Theta}(BrO_3^-/Br^-)$ = 1.423 V) is higher than that of hypobromous acid/bromide ($E^{\Theta}(HOBr/Br^-)$ = 1.331 V) (Bard et al., 1985), carbon materials that capable of reduce BrO_3^- is liable to reduce HOBr. Besides, activated carbon is often used to reduce chlorine to chloride, while chlorine has similar reactivity as HOBr.

As a new carbon material, graphene attracts enormous attention owing to its large surface area, unique two-dimensional unimolecular layer structure, high carrier mobility, excellent thermal conductivity etc. In our previous work, the photocatalytic decomposition of bromate was enhanced by graphene due to the improvement of photo-electron transportation (Huang et al., 2014). Moreover, graphene might react directly with pollutant instead of promoting electron transfer in some cases. It was found in chemical reduction of nitrobenzene by sulfide ion, the basal plane of graphene served as the conductor for the electron transfer, whilst the zig-zag edges served as the catalyst (Fu and Zhu, 2013). Another report proved Cr(VI) was indirectly reduced to Cr(III) by π electrons of rGO with the assistance of ligand and -COO groups on rGO surface (Ma et al., 2012). As the standard potential of Cr(VI)/Cr(III) at acidic pH ($E^{\Theta}(HCrO^-/Cr^{3+})$ = 1.35 V) is close to that of

hypobromous acid/bromide (E^{Θ}(HOBr/Br^-) = 1.331 V), HOBr is likely to be efficiently reduced by graphene. According to our knowledge, no research has been yet published on the reduction of bromine species by graphene or graphene oxide.

In this study, reduced graphene oxide (rGO) was prepared, characterized and applied to control the oxidation of Br^- to BrO_3^- in thermal/peroxymonosulfate (PMS) process. BrO_3^- is proved to be readily formed through radicals' oxidation, including hydroxyl radical (·OH) and sulfate radical ($SO4^{\cdot-}$) (Lutze et al., 2014). Thus the performance of rGO on inhibition of BrO_3^- formation was evaluated in bench-scale experiments in a wide range of pH at 5 - 9, temperature at 60 - 80 °C and rGO dosage at 5 - 35 mg/L. The decay of peroxymonosulfate was monitored, and the production of radicals was tested by chemical probes, respectively. Further, with the assistance of HOBr decay kinetics, the mechanism of bromate inhibition by rGO was discussed and elucidated.

2. Materials and methods

2.1 Materials

Potassium bromide (KBr, 99.8%) and graphite were purchased from Sinopharm Chemical Reagent Co., Ltd (China). Potassium peroxymonosulfate (PMS, $2KHSO_5 \cdot KHSO_4 \cdot K_2SO_4$, 99%) were purchased from J&K Scientific Ltd (China). Standards of bromide (Br^-, 1000 mg/L) and bromate (BrO_3^-, 1000 mg/L) for ion chromatography (IC) were obtained from Sigma Aldrich (USA). Solutions were prepared with Milli-Q water (≥ 18.2 MΩ•cm). Hypobromous acid (HOBr/OBr^-) was

prepared by Br_2, using $AgNO_3$ solution (20 g/L) to titrate the red-brown bromine until yellow at 4 °C, filtered by 0.45 μm membrane (Lahoutifard et al., 2002).

2.2 Preparation of graphene oxide (GO) and reduced graphene oxide (rGO)

Graphene oxide (GO) was synthesized following the modified Hummers' method (Pei et al., 2013). Briefly, the natural graphite was pre-oxidized by strong oxidizing agents (P_2O_5, $K_2S_2O_8$) in H_2SO_4 media. $KMnO_4$ and DI water are added successively and slowly with stirring and cooling in an ice-water mixed system. Then the mixture was re-oxidize using H_2O_2, then washed by 10% HCl aqueous solution and dried at 60 °C under a vacuum condition. Reduced grapheme oxide (rGO) was obtained by thermal treatment in tube furnace at 500 °C with N_2 protection for 2 h.

2.3 Characterization and analytical methods

Raman spectra of GO and rGO were collected on a confocal Raman spectrometer (Renishaw, UK) equipped with a 514 nm laser source. The X-ray diffraction (XRD) patterns were obtained on a X-ray diffractometer (D/max RBX, Japan) with Cu K radiation (λ = 1.5418 Å) at a scanning rate of 8 °/min in the 2θ range of 5 - 80 °. Surface elemental compositions of GO and rGO were determined by X-ray photoelectron spectroscopy (XPS, ESCALAB 250Xi, UK). Transmission electron microscopy (TEM) was operated on a JEOL 200CX TEM instrument. The thickness of rGO was determained on an atomic force microscope (AFM, Bruker Multi Mode 8, USA). The particle size distribution of rGO was determined by a laser particle size

analyzer (Malvern Mastersizer 3000E, UK). Solution pH was measured with a pH meter (METTLER TOLEDO FE20, USA). BrO_3^- and Br^- in water were quantified by an ion chromatograph (Metrohm MIC-2,Switzerland) with a 100 μL loop, and a conductivity measurement after suppression was used. The detection limit of BrO_3^- was 1.8 μg/L, which was 3.14 fold of the standard deviation of seven replicated analyses of 5 μg/L sample. Phenol was analyzed by a high-performance liquid chromatography (HPLC, Hitachi Primaide, Japan) equipped with a C8 analytical column (CNW Athena C8, China) using an isocratic elution of methanol/water (methanol content: 60%) detecting at 271 nm. Aqueous HOBr/OBr^- decomposition was quantified at 405 nm wavelength by 2,2-azino-bis (3-ethylbenzothiazoline)-6-sulfonic acid-diammonium salt (ABTS) photometric method. Peroxymonosulfate concentrations were determined by reacting PMS with $Fe(NH_4)_2(SO_4)_2$ at acidic pH (1 mol/L H_2SO_4) to form ferric ions, which further reacted with NH_4SCN to form colored $Fe(SCN)^{2+}$ to be read with a UV−vis spectrophotometer (METASH UV-5300PC, China) at a wavelength of 450 nm (Huang et al. 2002).

2.4 Experimental procedures

rGO was dosed in a range of 0 - 35 mg/L into 200 mL glass vials containing 20 μmol/L Br^- and 200 μmol/L peroxymonosulfate solutions on a magnetic stirrer. The temperature was kept by water-bath at 60 - 80 ± 1.5 °C. Solution pH was maintained by phosphate buffer solution (PBS) at a final concentration of 2 mmol/L.

Samples were collected at predetermined time and quickly cooled in ice water bath. One part of samples for ion chromatograph analysis was quenched by excessive sodium thiosulfate, stored at 4 °C for further analysis. The other part of samples were detected immediately for PMS and HOBr determination after sample collection. In the longevity test, the spent rGO were recovered by filtration from the reaction mixture, washed with DI water, and dried at 60 °C for repeated oxidation.

3. Results and discussions

3.1 Characterization of GO and rGO

Fig. 1(a) shows the XRD patterns of GO and rGO. The sharp peak at ca. $2\theta = 10.16$ ° is corresponding to the diffraction peak of GO, suggesting an interlayer spacing of 0.87 nm. After reduction of GO, the peak at 10.16 ° disappears and a weak peak at 25.30 ° emerges. The interlayer spacing decreases to ca. 0.35 nm due to the removal of oxygen-contained groups, indicating that rGO existed individually and highly disorderly (Yuan et al., 2011). Fig. 1(b) shows the Raman spectra of synthesized GO and rGO. The graphite lattice (G band) and graphite edge (D band) is at ca. 1590 cm^{-1} and 1330 cm^{-1}, respectively. This indicates the defects was created on the surface of GO and rGO during hydro-thermo synthesis. Standing for the ratio of defect to graphite (Lucchese et al., 2010), the I_D/I_G ratio for GO was determined to be 1.25, compared to 1.43 of I_D/I_G for rGO. This is similar to the previous report (Sun et al., 2012). The increased I_D/I_G value of rGO indicated more defects on rGO surface than that on GO, because of the removal of part oxygenated functional groups on GO

surface.. This was also partly proved by C : O ratio determined by XPS spectra. As shown in Fig. 1c and Fig. 1d, three peaks centered at 284.6 eV, 286.8 eV and 288.6 eV are observed of GO samples, corresponding to carbon atoms in aromatic rings (C-C/C=C), epoxy/ether (C-O-C) and carbonyl (C=O), respectively. After reduction, the amount of oxygenated functional groups decreases sharply, and consequently C : O ratio increases from 2.2 to 10.0 (Table S1).

Further, TEM image (Fig. 1e) shows an amorphous and disordered 2D-structure of rGO in nano-scale. The relatively weak diffraction rings of SAED pattern of rGO suggests a structure of monolayer that could be easily observed in Fig .1e. The thickness of rGO is determined to be ca. 1 nm by AFM, which is similar to the thickness of a single layered graphene. Therefore, the results of characterization strongly indicated that GO and rGO in nano-scale with a high defective structure were successfully synthesized in our experiments.

Fig. 1. (a) XRD patterns of GO and rGO; (b) Raman spectra of GO and rGO; (c) XPS spectra of GO and rGO; (d) C 1s XPS spectra of GO and rGO; (e) TEM image of rGO (Inset: selected-area electron diffraction pattern); (f) AFM image of rGO.

3.2 Effect of rGO on bromate inhibition

Fig. 2 shows the BrO_3^- formation kinetics during the thermal/PMS treatment in the presence of 0 - 35 mg/L rGO. The BrO_3^- concentration increased from zero to 1.6

μmol/L at 120 min in the absence of rGO. This coincides with the report that Br^- ion can be oxidized to BrO_3^- as a final product in sulfate radical treatment, i.e. UV/peroxydisulfate, Co/peroxymonosulfate (Li et al., 2015; Lutze et al., 2014). A significant decrease (ca. 67% - 100%) in the final concentration of BrO_3^- at 120 min was achieved, with addition of rGO in the range of 5 mg/L - 35 mg/L. Therefore, rGO has excellent performance on the inhibition of bromate formation. It's worth noting that GO has a similar but slightly lower performance than rGO (Fig. S1). rGO was then chosen in this study for simplicity.

Fig. 2. BrO_3^- formation during thermal/PMS process with different rGO dosage. (pH = 7.0, $[Br^-]_0$ = 20 μmol/L, $[PMS]_0$ = 200 μmol/L, activation temperature: 80 °C).

Fig. 3. Effect of temperature on BrO_3^- formation in thermal/PMS process. (pH = 7.0, $[Br^-]_0$ = 20 μmol/L, $[PMS]_0$ = 200 μmol/L , rGO dosage: 25 mg/L)

Fig. 4. Effect of pH on bromate formation during thermal/PMS process. ($[Br^-]_0$ = 20 μmol/L, $[PMS]_0$ = 200 μmol/L , rGO dosage: 25 mg/L, activation temperature: 80 °C).

Fig. 3 compares the effect of rGO on final BrO_3^- concentration at 2 h in the condition of various activation temperatures. As shown, the BrO_3^- was remarkably formed in the absence of rGO, reached a concentration of 0.28 ± 0.02, 1.31 ± 0.03 and 1.57 ±

213 0.09 μmol/L, at 60, 70 and 80 °C, respectively. Because higher temperature stimulates
214 the breaking down of PMS, leading to more $SO4^{\cdot -}$ and ·OH, and consequently
215 improve the formation of BrO_3^-. As expected, the performance of rGO was so stable
216 that 85%, 92% and 95% of BrO_3^- inhibition was achieved comparing with each blank
217 control at 60, 70 and 80 °C, respectively.
218 pH was always considered as an important factor affecting BrO_3^- formation in radical
219 oxidation process (Lutze et al., 2014; Von Gunten and Oliveras, 1998). As shown in
220 Fig. 4, the formation of BrO_3^- was increased with the pH increasing. In the absence of
221 rGO, the BrO_3^- concentration in pure thermal/PMS oxidation was 0.11 ± 0.01, 1.55
222 ± 0.02 and 2.45 ± 0.17 μmol/L at pH 5, 7 and 9, respectively. This is consistent
223 with the pronounced difference in the rate of PMS decay at different pH (Fig. S2).
224 Due to the base-catalyzed hydrolysis of persulfate (Furman et al., 2010), radical level
225 was probably elevated at alkaline pH, which consequently enhanced the producing of
226 BrO_3^-. However, BrO_3^- concentration decreased sharply when rGO was dosed. The
227 inhibition of produced BrO_3^- was 100%, 94% and 90% at pH 5, 7 and 9, respectively.
228 The stable performance of rGO was further testified in longevity studies, where the
229 suppressing efficacy of bromate formation dropped slightly from 94.9% at 1st run to
230 90.2% at 4th run (Fig. S3). Correspondingly, the C : O ratio dropped from 10.0 of
231 fresh rGO to 6.8 of used rGO after 4th run (Fig. S4), indicating that the rGO surface
232 was oxidized in thermal/PMS treatment. Besides the chemical structure, the diameter
233 of particle size is commonly considered as another important factor affecting the
234 performance of carbon materials. Although the thickness of rGO was in the magnitude

of nano-meter (Fig. 1e, 1f), the particle size distribution of this sort of thin layered material was in the magnitude of micro-meter with an average of 28.6 μm and a 90% percentile of 40.1 μm (Fig. S5). This is similar to the diameter of powder activated carbons, while graphene has a much better inhibitory effect than activated carbons (Humbert et al., 2008; Jakob et al., 2012; Siddiqui et al., 1996). Thus, owing to its unique chemical structure, rGO was proved to have excellent and stable performance on BrO_3^- inhibition in thermal/PMS process, almost irrelevance of pH and temperature.

3.3 The influence of rGO on PMS activation and organics degradation

Since BrO_3^- is proved to be oxidized from Br^- by radicals, one may propose that rGO interrupts the generation of radicals in thermal/PMS process, leading to the inhibition of BrO_3^-. Fig. 5 shows the natural logarithm of the PMS concentration at each time to the initial concentration (C/C_0) with rGO addition. The almost linear relationship between $\ln(C/C_0)$ and time indicated the decay of PMS followed pseudo-first order kinetics well ($R^2 > 0.977$). The apparent constant (k_{obs}), which was the slope of each line, was slightly increased from 0.0162 ± 0.0013 min^{-1} in the absence of rGO, to 0.0165 ± 0.0010 min^{-1} - 0.0200 ± 0.0010 min^{-1} in the presence of 5 - 35 mg/L rGO (Fig. 5 inset). This promoting effect of rGO on PMS decomposition is similar with previous work (Sun et al., 2012). In Sun's study, the catalytic activation of PMS by rGO is more obvious than the results shown in this experiment, probably due to the higher dosage of rGO (100 - 500 mg/L) that is 2.86 - 100 times more than that in

256 current case (5 - 35 mg/L).

257 To further confirm whether the radical levels were changed by dosing rGO, phenol
258 was chosen as a model compound to evaluate the oxidation capacity of
259 rGO-thermos/PMS process. rGO has little adsorption capacity for anionic pollutants
260 such as phenolic compound, which is due to their negatively charged surface at
261 neutral pH. Accordingly, phenol was used as a model probe for the exclusion of
262 adsorption on rGO. As shown in Fig. 6, phenol neither degraded in hot water at 80 °C
263 nor being absorbed by rGO in 60 min. In addition, rGO slightly accelerated the
264 removal of phenol with a pseudo-first-order rate constant of 0.0204 $\pm$ 0.0022 min^{-1},
265 as compared with 0.0157 $\pm$ 0.0012 min^{-1} in thermal/PMS treatment. This is in
266 accordance with the moderate enhancement of PMS decay as shown in Fig. 5. Hence
267 the degradation of phenol confirmed the radical concentration was not lowered but
268 slightly raised after dosing rGO. In addition, the radical species distribution, i.e. the
269 ratio of $SO4^{\cdot -}$ and ·OH, might be altered insignificantly, as comparing the patterns of
270 HPLC chromatograms during phenol degradation. As shown in Fig. S6, in both
271 rGO-thermo/PMS and thermos/PMS treatment, there are two major characteristic
272 peaks, one is for phenol with retention time at ca. 4.5 min, and another for its
273 byproduct with retention time at ca. 2.5 min. Along with the proceeding of reaction,
274 the peak of phenol gradually decreased with its degraded product increasing. Such
275 pattern was almost same between rGO-thermo/PMS and thermos/PMS treatment.

276

277 Fig. 5. Decay of PMS in thermal/PMS process in the presence of rGO (Inset: the

pseudo-first-order rate constants, pH = 7.0, $[PMS]_0$ = 200 μmol/L, activation temperature: 80 °C).

Fig. 6. The degradation kinetics of phenol in rGO, PMS and thermal/PMS treatment. (pH = 7.0, $[PMS]_0$ = 200 μmol/L, $[Phenol]_0$ = 3 mg/L, rGO dosage: 25 mg/L, activation temperature: 80 °C)

3.4 Path block of bromate formation from HOBr via rGO

Now that the addition of rGO didn't affect the oxidants decay and subsequent radical generation significantly in thermal/PMS, one possible route for rGO reaction is reacting with bromine species, leading to the block of formation path of BrO_3^-. The possibility of adsorption or reaction of rGO with BrO_3^- and Br^- was firstly ruled out, for the concentration of BrO_3^- and Br^- was remained nearly constant in the presence of rGO (Fig. S7). This is probably due to the pHzpc of rGO at 6.2 (Lingamdinne et al., 2017), which led to the negative surface of rGO at the current pH (5-9).

In contrast with BrO_3^- and Br^-, HOBr was prone to react with rGO. As shown in Fig. 7, the decay of HOBr was fast and followed pseudo-first order kinetics (R^2>0.97). The apparent pseudo-first order rate constant (k_{obs}) was 0.022 ± 0.001, 0.036 ± 0.001 and 0.041 ± 0.002 min^{-1}, with $[HOBr]_0$ at 2.5, 5 and 10 μmol/L, respectively, whilst no self-decay of HOBr occurred at room temperature within the duration of experiments (Fig. S8). No bromate was determined after reduction of HOBr. The concentration of bromide in 2.5 μmol/L HOBr solution was determined after the

299 decay completed (at 60 min). The removed HOBr in solution was 1.51 ± 0.03
300 mmol/L that is nearly equal to the increased Br^- ion (1.60 ± 0.07 mmol/L). This
301 strongly suggested that HOBr was reduced to bromide ion by rGO.
302 The masking of hypobromous acid has been proven an effective strategy to minimize
303 BrO_3^- formation. Here the k_{obs} of rGO is chosen then to be compared with other
304 inhibitions measures applying H_2O_2 and ammonia. The decay of hypobromous acid in
305 H_2O_2/O_3 could be evaluated as : $d[HOBr]_{tot}/dt = k_{OBr\cdot,H2O2}[OBr^-][H_2O_2] + k_{HOBr\cdot,HO2^-}$
306 $[HOBr][HO_2^-] = k_{obs}[HOBr]_{tot}$ (Von Gunten and Oliveras, 1997). Given a dose of 30
307 μmol/L H_2O_2 in ozonation (H_2O_2:O_3 = 1:1, 1.5 mg/L O_3), $k_{OBr\cdot,H2O2}$ = (1.2 ± 0.2) ×
308 10^6 M^{-1} s^{-1}, $k_{HOBr\cdot,HO2^-}$ = (7.6 ± 1.3) × 10^8 M^{-1} s^{-1} and the hydrolysis of HOBr and
309 H_2O_2 (Eq.1 - 2, Table 1), the k_{obs} at pH 7 would be 0.02 min^{-1}, which is close to the
310 results of this experiment. The scavenging of hypobromous acid by ammonia follows
311 Eq. 3 - 4 (Table 1), from which the decay of HOBr could be written as $d[HOBr]_{tot}/dt =$
312 $k_{HOBr\cdot,NH3}[HOBr][NH_3] = k_{obs}[HOBr]_{tot}$ (Pinkernell and von Gunten, 2001). Given a
313 common dose of 0.1 mg/L ammonia in ozonation, the k_{obs} at pH 7 would be 0.044
314 min^{-1}, which is also close to the results of this experiment. Therefore, the apparent
315 constant (k_{obs}) of HOBr decay inducing by rGO is comparable to that by dosing H_2O_2
316 or ammonia, which makes the inhibition plausible and explainable.
317
318 Table 1 Reactions and rate constants for hypobromous acid and hydrogen peroxide in
319 aqueous solutions
320

Although the detailed mechanisms remains unknown, the surface defects, i.e. the zigzag edges of rGO with high chemical reactivity may play key role in the direct reduction of HOBr to Br^- due to the nonbonding π-electron. Surface defects on graphene oxide could be active sites for oxygen reduction reaction (Jia et al., 2016; Zhao et al., 2015; Zhao et al., 2016). According to our knowledge, similar mechanism was proposed in graphene involved reactions, including the activation of PMS by rGO (Sun et al., 2012), the direct reduction of Cr(VI) to Cr(III) by ethylenediamine-rGO (Ma et al., 2012), and the GO facilitate reduction of nitrobenzene by sulfide (Fu and Zhu, 2013). An indirect evidence in our experiment is the lower inhibition capacity achieved by GO than rGO (Fig. S1), where GO with lower I_D/I_G has less defects than rGO (Fig. 1b).

For application view, since the masking of HOBr by rGO is relevant to its chemical structures instead of oxidation process, it is promising that rGO performs well in oxidation processes that BrO_3^- readily forms. As shown in Fig. 8, a significant inhibition of BrO_3^- was achieved at pH 5.3 - 8.8. So this good effect irrespective of oxidation procedure again support the proposed mechanisms that rGO suppress the formation of BrO_3^- by reducing HOBr to Br^-.

Fig. 7. Kinetics of HOBr degradation by rGO (Inset: pseudo-first order kinetics fitting, pH = 7.0, rGO dosage: 25 mg/L, activation temperature: 25 °C)

Fig. 8. Inhibition of bromate formation by rGO in batch ozonation treatment at

various pH (rGO dosage: 25 mg/L, $[Br^-]_0$ = 0.5 mg/L, $[O_3]_0$ = 5 mg/L).

4. Conclusion

This work verified the effect of rGO on the inhibition of BrO_3^- via reacting with HOBr to Br^- in the thermal activated PMS process. Reduced graphene oxide (rGO) was successfully synthesized through hydro-thermal methods. The effect of rGO on the decomposition rate of PMS, the removal kinetics of phenol as target pollutant and the alteration patterns of HPLC chromatograms in thermal/PMS were thoroughly studied. There were tiny differences between thermal/PMS and rGO-thermal/PMS process under the dosage of 5 - 35 mg/L rGO. Interestingly, the formed BrO_3^- was significantly lowered with the addition of rGO in a wide range of pH at 5 - 9 and activation temperature at 60 – 80 °C. Being compared with the behavior of rGO on degradation of target pollutant, this phenomenon strongly indicated that neither PMS nor secondary radicals, but bromine species were prone to react with rGO. The quick reduction of HOBr to Br^- by rGO was then experimented and proved at room temperature, of which the pseudo-first order rate was in the same order with that achieved by applying H_2O_2 and ammonia at typical dosage. In addition, no abatement of BrO_3^- and Br^- was made for rGO adsorption. Thus, the role of rGO on masking HOBr was then proved. Further, similar excellent inhibiting effect of BrO_3^- was observed in rGO/ozonation. So addition of rGO in tens of mg/L is a promising measure to avoid the formation of unwanted bromine species in advanced oxidation process. In comparison with other HOBr masking measures, i.e. ammonia and H_2O_2,

364 it shows some unique benefits, such as insignificant influence of oxidation procedure,
365 adsorptive removal of cationic organics and avoiding formation of unwanted
366 chemicals.

367 **Acknowledgment**

368 This study was partially supported by the National Science Foundation Project of
369 China (No. 51678351) and the Program for Innovative Research Team in University
370 (No. IRT13078).

371 **References**

372 Bao, M. L., Griffini, O., Santianni, D., Barbieri, K., Burrini, D., Pantani, F., 1999. Removal of
373 bromate ion from water using granular activated carbon. Water Research 33 (13), 2959-2970.
374 Bard, A. J., Parsons, R., Jordan, J., 1985. Standard potentials in aqueous solution (Vol. 6). CRC
375 press.
376 Berne, F., Chasson, G., Legube, B., 2004. Effect of Addition of ammonia on the bromate
377 formation during ozonation. Ozone: Science and Engineering 26 (3), 267-276.
378 Bull, R. J., Kolisetty, N., Zhang, X., Muralidhara, S., Quiñones, O., Lim, K. Y., Guo, Z., Cotruvo,
379 J. A., Fisher, J. W., Yang, X., Delker, D., Snyder, S. A., Cummings, B. S., 2012. Absorption
380 and disposition of bromate in F344 rats. Toxicology 300 (1–2), 83-91.
381 Fang, J. Y., Shang, C., 2012. Bromate formation from bromide oxidation by the UV/persulfate
382 process. Environmental Science and Technology 46 (16), 8976-8983.
383 Fu, H., Zhu, D., 2013. Graphene oxide-facilitated reduction of nitrobenzene in sulfide-containing

aqueous solutions. Environmental Science and Technology 47 (9), 4204-4210.

Furman, O. S., Teel, A. L., Watts, R. J., 2010. Mechanism of base activation of persulfate. Environmental Science and Technology 44 (16), 6423-6428.

Hofmann, R., Andrews, R. C., 2007. Potential side effects of using ammonia to inhibit bromate formation during the ozonation of drinking water. Journal of Environmental Engineering and Science 6 (6), 739-743.

Huang, K. C., Couttenye, R. A., Hoag, G. E., 2002. Kinetics of heat-assisted persulfate oxidation of methyl tert-butyl ether (MTBE). Chemosphere 49 (4), 413-420.

Huang, W. J., Cheng, Y. L., 2008. Effect of characteristics of activated carbon on removal of bromate. Separation and Purification Technology 59 (1), 101-107.

Huang, X., Gao, N., Deng, Y., 2008. Bromate ion formation in dark chlorination and ultraviolet/chlorination processes for bromide-containing water. Journal of Environmental Sciences-China 20 (2), 246-251.

Huang, X., Wang, L., Zhou, J., Gao, N., 2014. Photocatalytic decomposition of bromate ion by the UV/P25-graphene processes. Water Research 57, 1-7.

Humbert, H., Gallard, H., Suty, H., Croué, J. P., 2008. Natural organic matter (NOM) and pesticides removal using a combination of ion exchange resin and powdered activated carbon (PAC). Water Research 42 (6), 1635-1643.

Jakob, L., Hartnik, T., Henriksen, T., Elmquist, M., Brändli, R. C., Hale, S. E., Cornelissen, G., 2012. PAH-sequestration capacity of granular and powder activated carbon amendments in soil, and their effects on earthworms and plants. Chemosphere 88 (6), 699-705.

Jia, Y., Zhang, L., Du, A., Gao, G., Chen, J., Yan, X., Brown, C. L., Yao, X., 2016. Defect

graphene as a trifunctional catalyst for electrochemical reactions. Advanced Materials 28 (43), 9532-9538.

Lahoutifard, N., Lagrange, P., Lagrange, J., Scott, S. L., 2002. Kinetics and mechanism of nitrite oxidation by HOBr/BrO-in atmospheric water and comparison with oxidation by HOCl/ClO. The Journal of Physical Chemistry A 106 (49), 11891-11896.

Le Roux, J., Gallard, H., Croué, J. P., 2012. Formation of NDMA and halogenated DBPs by chloramination of tertiary amines: the influence of bromide ion. Environmental Science and Technology 46 (3), 1581-1589.

Li, W., Lu, X., Xu, K., Qu, J., Qiang, Z., 2015. Cerium incorporated MCM-48 (Ce-MCM-48) as a catalyst to inhibit bromate formation during ozonation of bromide-containing water: Efficacy and mechanism. Water Research 86, 2-8.

Li, Z., Chen, Z., Xiang, Y., Ling, L., Fang, J., Shang, C., Dionysiou, D. D., 2015. Bromate formation in bromide-containing water through the cobalt-mediated activation of peroxymonosulfate. Water Research 83, 132-140.

Lingamdinne, L. P., Choi, Y. L., Kim, I. S., Yang, J. K., Koduru, J. R., Chang, Y. Y., 2017. Preparation and characterization of porous reduced graphene oxide based inverse spinel nickel ferrite nanocomposite for adsorption removal of radionuclides. Journal of Hazardous Materials 326, 145-156.

Liu, C., Von Gunten, U., Croue, J. P., 2012. Enhanced bromate formation during chlorination of bromide-containing waters in the presence of CuO: catalytic disproportionation of hypobromous acid. Environmental Science and Technology 46 (20), 11054-11061.

Lucchese, M. M., Stavale, F., Ferreira, E. M., Vilani, C., Moutinho, M. V. O., Capaz, R. B., Achete,

C. A., Jorio, A., 2010. Quantifying ion-induced defects and Raman relaxation length in graphene. Carbon 48 (5), 1592-1597.

Lutze, H. V., Bakkour, R., Kerlin, N., von Sonntag, C., Schmidt, T. C., 2014. Formation of bromate in sulfate radical based oxidation: mechanistic aspects and suppression by dissolved organic matter. Water Research 53, 370-377.

Ma, H. L., Zhang, Y., Hu, Q. H., Yan, D., Yu, Z. Z., Zhai, M., 2012. Chemical reduction and removal of Cr (VI) from acidic aqueous solution by ethylenediamine-reduced graphene oxide. Journal of Materials Chemistry 22 (13), 5914-5916.

Nie, Y., Hu, C., Yang, L., Hu, J., 2013. Inhibition mechanism of BrO_3^- formation over MnO_x/Al_2O_3 during the catalytic ozonation of 2,4-dichlorophenoxyacetic acid in water. Separation and Purification Technology 117 (39), 41-45.

Pei, F., Liu, Y., Xu, S., Lü, J., Wang, C., Cao, S., 2013. Nanocomposite of graphene oxide with nitrogen-doped TiO_2 exhibiting enhanced photocatalytic efficiency for hydrogen evolution. International Journal of Hydrogen Energy 38 (6), 2670-2677.

Pinkernell, U., von Gunten, U., 2001. Bromate minimization during ozonation: mechanistic considerations. Environmental Science and Technology 35 (12), 2525-2531.

Siddiqui, M., Zhai, W., Amy, G., Mysore, C., 1996. Bromate ion removal by activated carbon. Water Research 30 (7), 1651-1660.

Soltermann, F., Abegglen, C., Tschui, M., Stahel, S., von Gunten, U., 2017. Options and limitations for bromate control during ozonation of wastewater. Water Research.

Sun, H., Liu, S., Zhou, G., Ang, H. M., Tadé, M. O., Wang, S., 2012. Reduced graphene oxide for catalytic oxidation of aqueous organic pollutants. ACS Applied Materials and Interfaces 4

(10), 5466-5471.

Von Gunten, U., Hoigne, J., 1994. Bromate formation during ozonization of bromide-containing waters: interaction of ozone and hydroxyl radical reactions. Environmental Science and Technology 28 (7), 1234-1242.

Von Gunten, U., Oliveras, Y., 1997. Kinetics of the reaction between hydrogen peroxide and hypobromous acid: implication on water treatment and natural systems. Water Research 31 (4), 900-906.

Von Gunten, U., Oliveras, Y., 1998. Advanced oxidation of bromide-containing waters: bromate formation mechanisms. Environmental Science and Technology 32 (1), 63-70.

Wu, Y., Wu, C., Wang, Y., Hu, C., 2014. Inhibition of Nano-Metal Oxides on Bromate Formation during Ozonation Process. Ozone: Science and Engineering 36 (6), 549-559.

Yuan, W., Li, B., Li, L.,2011. A green synthetic approach to graphene nanosheets for hydrogen adsorption. Applied Surface Science 257 (23), 10183-10187.

Zhao, H., Sun, C., Jin, Z., Wang, D. W., Yan, X., Chen, Z., Zhu, G., Yao, X., 2015. Carbon for the oxygen reduction reaction: a defect mechanism. Journal of Materials Chemistry A 3 (22), 11736-11739.

Zhao, X., Zou, X., Yan, X., Brown, C. L., Chen, Z., Zhu, G., Yao, X., 2016. Defect-driven oxygen reduction reaction (ORR) of carbon without any element doping. Inorganic Chemistry Frontiers 3 (3), 417-421.

Table 1 Reactions and rate constants for hypobromous acid and hydrogen peroxide in aqueous solutions

(1) $HOBr \leftrightarrow OBr^- + H^+$	1.26×10^{-9} mol/L
(2) $H_2O_2 \leftrightarrow HO_2^- + H^+$	2.50×10^{-12} mol/L
(3) $NH_4^+ \leftrightarrow NH_3 + H^+$	5.0×10^{-10} mol/L
(4) $HOBr + NH_3 \rightarrow NH_2Br + H_2O$	7.5×10^{7} L/(mol·s)

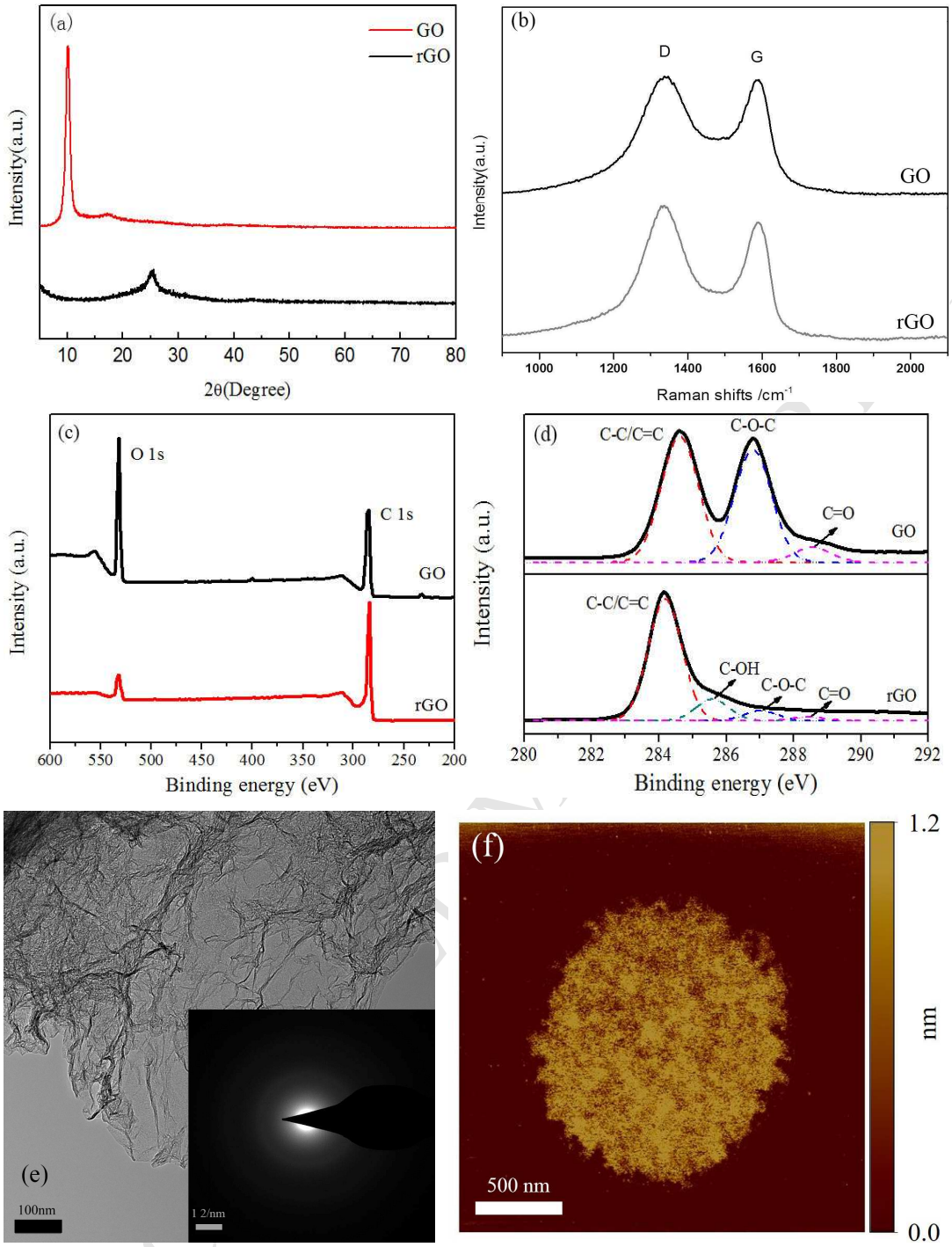

Fig. 1. (a) XRD patterns of GO and rGO; (b) Raman spectra of GO and rGO; (c) XPS spectra of GO and rGO; (d) C 1s XPS spectra of GO and rGO; (e) TEM image of rGO (Inset: selected-area electron diffraction pattern); (f) AFM image of rGO.

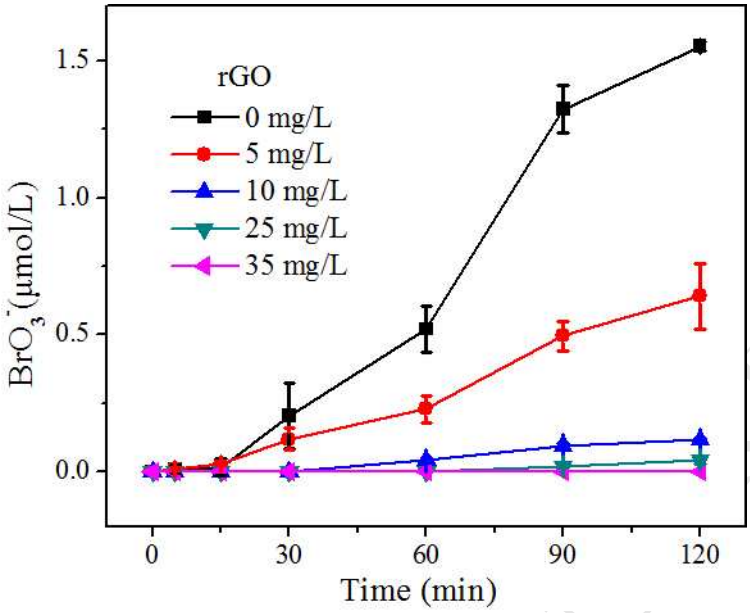

Fig. 2. BrO_3^- formation during thermal/PMS process with different rGO dosage. (pH = 7.0, $[Br^-]_0$ = 20 μmol/L, $[PMS]_0$ = 200 μmol/L, activation temperature: 80 °C).

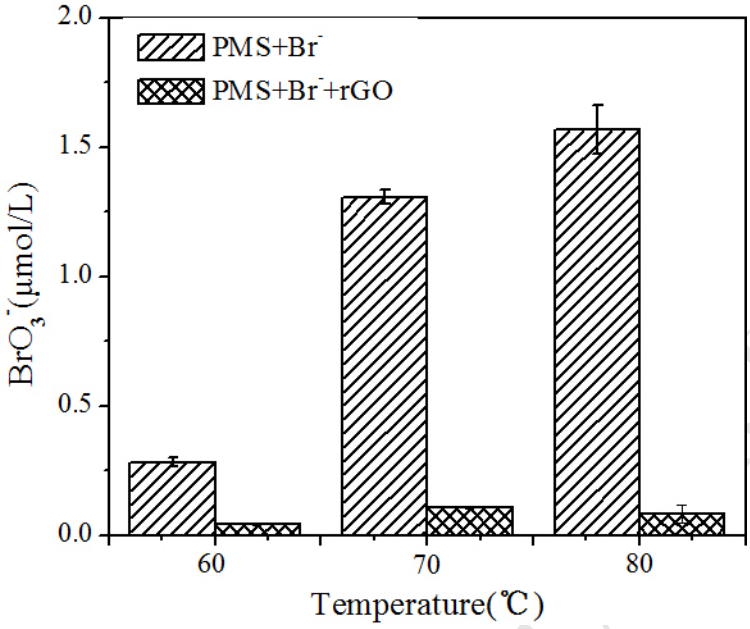

Fig. 3. Effect of temperature on BrO_3^- formation in thermal/PMS process. (pH = 7.0, $[Br^-]_0$ = 20 μmol/L, $[PMS]_0$ = 200 μmol/L , rGO dosage: 25 mg/L)

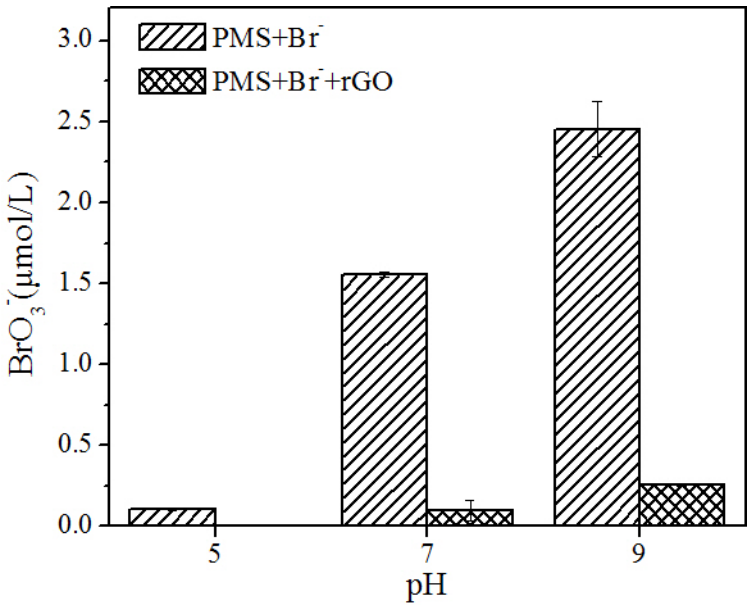

Fig. 4. Effect of pH on bromate formation during thermal/PMS process. ($[Br^-]_0$ = 20 μmol/L, $[PMS]_0$ = 200 μmol/L , rGO dosage: 25 mg/L, activation temperature: 80 °C).

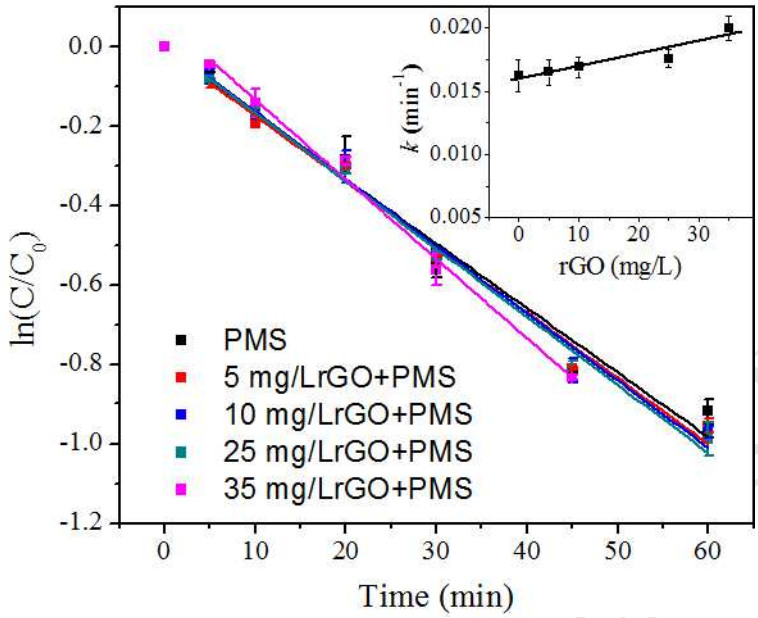

Fig. 5. Decay of PMS in thermal/PMS process in the presence of rGO (Inset: the pseudo-first-order rate constants, pH = 7.0, $[PMS]_0$ = 200 μmol/L, activation temperature: 80 °C).

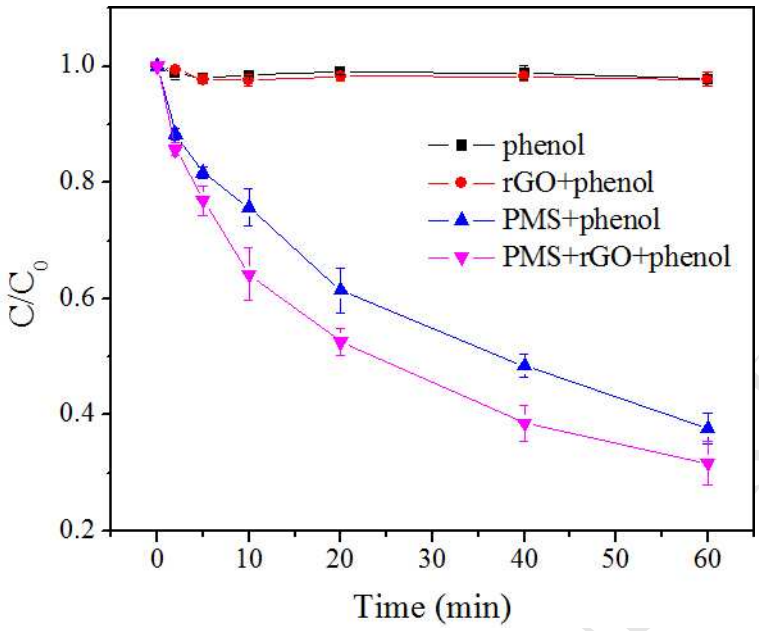

Fig. 6. The degradation kinetics of phenol in rGO, PMS and thermal/PMS treatment. (pH = 7.0, $[PMS]_0$ = 200 μmol/L, $[Phenol]_0$ = 3 mg/L, rGO dosage: 25 mg/L, activation temperature: 80 °C)

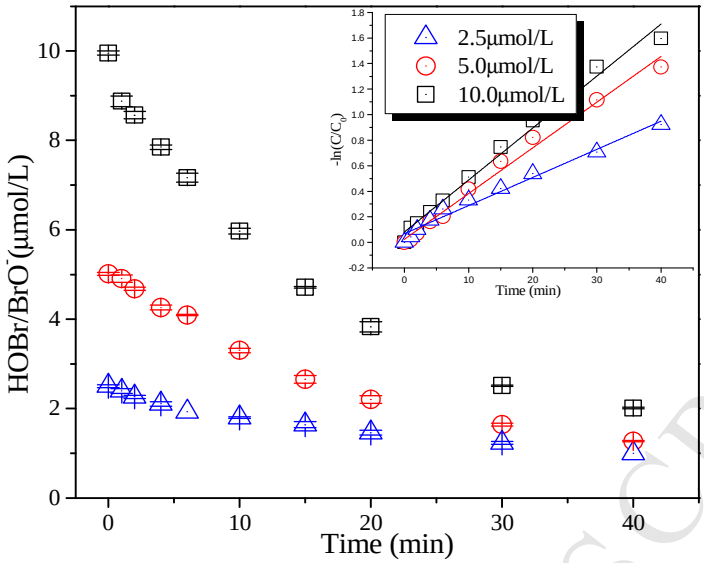

Fig. 7. Kinetics of HOBr degradation by rGO (Inset: pseudo-first order kinetics fitting, pH = 7.0, rGO dosage: 25 mg/L, activation temperature: 25 °C)

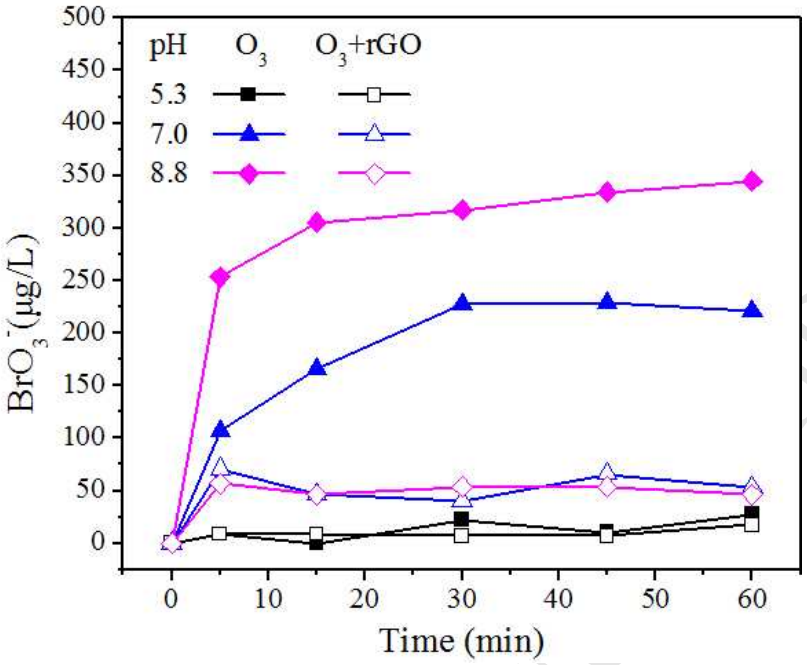

Fig. 8. Inhibition of bromate formation by rGO in batch ozonation treatment at various pH (rGO dosage: 25 mg/L, $[Br^-]_0$ = 0.5 mg/L, $[O_3]_0$ = 5 mg/L).

- Reduced graphene oxide (rGO) is firstly used to inhibit BrO_3^- formation.
- rGO suppress BrO_3^- formation effectively in thermal/PMS and ozonation.
- The decay of PMS and generation of radicals are altered insignificantly by rGO.
- rGO could reduce hypobromous acid (HOBr) to Br^-.